Electronic and magnetic properties of disordered Fe–Cr alloys using different electronic structure methods

2008 J. Phys.: Condens. Matter 20 445201

(http://iopscience.iop.org/0953-8984/20/44/445201)

IOP PUBLISHING JOURNAL OF PHYSICS: CONDENSED MATTER

J. Phys.: Condens. Matter **20** (2008) 445201 (11pp) doi:10.1088/0953-8984/20/44/445201

Electronic and magnetic properties of disordered Fe–Cr alloys using different electronic structure methods

Kartick Tarafder[1,2], Subhradip Ghosh[4], Biplab Sanyal[1], Olle Eriksson[1], Abhijit Mookerjee[1,5] and Atisdipankar Chakrabarti[3]

[1] Division of Materials Theory, Department of Materials Science, University of Uppsala, Box-530 SE-75121, Uppsala, Sweden
[2] Department of Materials Science, S N Bose National Center for Basic Sciences, JD-III, Salt Lake City, Kolkata 700098, India
[3] RK Mission Vivekananda Centenary College, Rahara, Kolkata 700118, India
[4] Department of Physics, Indian Institute of Technology, Guwahati 781039, India

E-mail: abhijit@bose.res.in

Received 26 June 2008, in final form 24 August 2008
Published 30 September 2008
Online at stacks.iop.org/JPhysCM/20/445201

Abstract

In this paper we have studied the electronic structure of bcc Fe_xCr_{1-x} alloys in the ferromagnetic phase using three different techniques: augmented space recursion coupled with tight-binding linearized muffin-tin orbitals (TB-LMTO-ASR), the coherent potential approximation based on the Korringa–Kohn–Rostocker method (KKR-CPA) and the special quasi-random structure technique linked with the projector augmented wave (PAW-SQS). The aim was to provide a comparison between the different methods and examine their strengths and weaknesses vis-à-vis one another.

(Some figures in this article are in colour only in the electronic version)

1. Introduction

Scientific literature lists several calculational methods to deal with the electronic structure and phase stability of disordered alloys. These include both methods for solving the related Kohn–Sham equation and also different techniques for dealing with the effect of disorder-induced fluctuations in the configuration space of random variables of the Hamiltonian. Each method claims superiority for itself. For comparison, therefore, it is important to select the most successful techniques available and apply them on an alloy system where there has already been extensive experimental studies. This will allow us to carry out calculations using these techniques with controlled and comparable approximations: something which cannot be ensured in diverse works by different groups. Such a study will give us a clear picture of the comparative strengths and weaknesses of these methods vis-à-vis one another. An alloy system, like Fe_xCr_{1-x}, is an excellent choice on which to carry out such a comparative analysis. This is the basic aim of the work presented here.

The reason for the extensive interest in FeCr alloys is in its various possible practical uses. Industrial steels with chemical compositions based on an FeCr matrix with Cr concentrations ranging from 2 to 20 at.% are possible candidates for the design of structural components in advanced nuclear energy installations like the Generation IV and fusion reactors [1, 2]. Of the various multilayer systems which show oscillatory exchange coupling of ferromagnetic films across non-ferromagnetic spacer layers, Fe/Cr multilayers have shown the greatest promise [3]. It has been felt that, in order to understand multilayers, we must first attempt to understand binary inter-metallic compounds as well as random binary alloys: the former, since in the B2 structure they are naturally occurring models of single atomic multilayers, and the latter, in particular, to give insight into disordering at the multilayer interfaces [4].

There are ample experimental investigations on this alloy system. These include studies on structural phase stability

[5] Permanent address: Advanced Materials Research Unit, S N Bose National Center for Basic Sciences, JD-III, Salt Lake City, Kolkata 700098, India.

and phase diagrams [5–13], spinodal decomposition [14, 15], structural studies from x-ray scattering [16, 17], inelastic neutron scattering [18, 19], Mössbauer [20–24], heat capacity [25–27], thermopower [28], the magnetic phase stability [29] and magnetic phases of Fe_xCr_{1-x} alloys [30–40]. They provide a variety of information, e.g. variation of magnetization with band filling [41], moment distribution in dilute Fe-based alloys [42], composition dependence of high-field susceptibility [43], low-temperature specific heat [44] and resistivity anomaly [45].

Theoretical investigations have been carried out on the phase stability of Fe_xCr_{1-x} alloys [46–53]. There have been several calculations on ordered inter-metallic FeCr in the B2 structure using standard electronic structure methods [54–57]. Studies on FeCr in the σ phase have also been reported [58].

Magnetism in this alloy has been studied by the spin-polarized KKR-CPA method by many authors [56–59]. Butler *et al* [60] have studied the GMR effect in the concentration range of $(0.5 < x < 0.1)$ and the antiferro-to ferromagnetic transition at the critical concentration of $x = 0.3$. Dederichs *et al* [61] have discussed the Slater–Pauling curves of Fe_xCr_{1-x}. Kulikov *et al* [62] have shown that body-centred cubic Fe moments are fairly independent of Cr concentration, while the opposite is true for Cr.

Jiang *et al* [63] have studied the local environment effect on the formation enthalpy, magnetic moments, equilibrium lattice parameter and bond lengths using special quasi-random structure (SQS), a concept proposed by Zunger *et al* [64]. With a 16-atom SQS supercell they have shown that, even for a lattice-matched system like Fe_xCr_{1-x}, the average Cr–Cr, Cr–Fe and Fe–Fe bond lengths are quite different. For magnetic moment calculations they have obtained reliable results in the concentration range of $x > 0.3$. Olsson *et al* [65] have also studied the anomalous stability of Fe-rich Fe_xCr_{1-x} using both exact muffin-tin orbitals coherent potential approximation (EMTO-CPA) and the projector augmented wave SQS (PAW-SQS). These authors have scanned a much wider composition range using a 128-atom SQS supercell.

The foregoing discussion and the extensive references justify our choice of the Fe_xCr_{1-x} alloy system for our comparative study. We shall identify a few of the first-principles electronic structure methods for disordered alloys which we believe to be the most accurate and make a comparative analysis of results obtained for Fe_xCr_{1-x}. A comparative study of different properties like density of states and magnetic moments have not been studied using electronic structure methods coupled with different approximations dealing with disorder. Our work will provide insights into the advantages and drawbacks of these techniques and give us confidence in their use for future studies on different alloy systems.

We have identified three electronic structure methods as being successful for disordered substitutional binary alloys: the Korringa–Kohn–Rostocker-based mean-field coherent potential approximation (KKR-CPA) [66], the projector augmented-wave-based supercell calculations on special quasi-random structures (PAW-SQS) [64] and the tight-binding linear muffin-tin-orbitals-based augmented space recursion (TB-LMTO-ASR) [67].

The KKR and its linear version, the LMTO, both based on a muffin-tin modelling of the effective electron–ion potential, are among the accurate techniques for the solution of the Kohn–Sham equation. The form of the secular equation makes them suitable for the study of random substitutional alloys, where the disorder-induced scattering is *local*. Of course, LMTO, being a linearized approximation to the KKR, is expected to be less accurate. However, if the energy window around the linearization energy nodes is not too large, the LMTO estimates energies with reasonable tolerances. Unless we are interested in estimating very small energy differences or over large energy windows, the LMTO is good enough and has the great advantage that its secular equation is an eigenvalue problem rather than the more complicated functional equation of the KKR. In the PAW, as implemented in the VASP code [68]–[70], the electron–ion potential is described by a marriage between the pseudo-potential and features of the augmented plane wave (APW) methods [70, 71].

Methods to deal with disorder fall into three categories. In the first category belongs the single-site mean-field CPA. This approximation has been eminently successful in dealing with a variety of disordered systems. Of all the single-site approximations, the CPA alone maintains the essential Herglotz[6] analytical properties and lattice translational symmetry of the averaged Green function. However, whenever there is either strong scattering due to disorder-induced configuration fluctuations, as in dilute, split-band alloys or when local environment effects like short-ranged ordering, clustering and segregation, or local lattice distortions due to size mismatch of the constituent atoms become important, the single-site-based CPA becomes inadequate.

In the second category belong the generalizations of the CPA, of which the augmented-space-based methods: the itinerant CPA (ICPA) [72] and the augmented space recursion [73] (ASR), are foremost. They too not only retain the necessary analytic (Herglotz) properties and lattice translational symmetry of the averaged Green function, as the CPA does, but also properly incorporate local environment effects.

In the third category belong the supercell-based calculations. Zunger [64] suggested that, if we construct a supercell and populate its lattice points randomly by the constituents so as to mimic the concentration correlations in the random alloy, a single calculation with this superlattice should approximate the configuration average in the infinite random system. This special quasi-random structure (SQS) approach has been used to incorporate short-ranged order and local lattice distortions in alloy systems. Certainly, in the limit of a very large supercell this statement is the *theorem of spatial ergodicity*. This theorem provides the explanation of why a single experiment on global property of a bulk material most often produces the configuration averaged result, provided the property we are looking at is *self-averaging*. How far this approach is accurate with a small cluster of, say, 16 atoms, is *a priori* uncertain. We shall use the SQS method for averaging as well and compare this with our mean-field and ASR results.

[6] A complex function $f(z)$ is called Herglotz if (a) its singularities lie on the real z axis, (b) $\mathrm{Sgn}(\mathrm{Im}\, f(z)) = -\mathrm{Sgn}(\mathrm{Im}\, z)$ and (c) $f(z) \sim 1/z$ as $z \to \pm\infty + \mathrm{i}0$.

Before we proceed further, we should note that all three methods, described earlier, to deal with disorder are essentially real space approaches. The disorder is substitutional and *at a site*. There is a fourth technique recently introduced based on a reciprocal-space renormalization method: the non-local CPA. The basic technique was introduced by Jarrel and Krishnamurthy [74] and applied to CuZn alloys by Rowlands *et al* [75]. The method is capable of taking into account environmental effects and short-ranged ordering. As expertise in this method was not available to us we could not include it in this work. Once work on FeCr is available using this technique, it would be interesting to compare those results with ours.

A systematic comparison between these calculations will allow us to ascertain, for example, whether the CPA is indeed inadequate in some situations and how far the augmented-space-based techniques or the SQS improve matters.

2. Computational details

The KKR-CPA calculations were based on the total energy formalism by Johnson *et al* [76] as implemented in the MECCA code [77, 78]. The 3d states of Fe and Cr were put in the valence band. All calculations were done using the atomic sphere approximation (ASA) with equal-sized Fe and Cr atomic spheres. All angular momentum expansions include up to $\ell_{\max} = 3$. A semicircular contour in the complex plane with 20 points was used to integrate the Green function over energy. At each energy, the Brillouin zone integration was performed by a special k-point $20 \times 20 \times 20$ mesh.

For recursion in augmented space we have checked the convergence of the Fermi energy and the first three moments of the density of states with both the number of nearest-neighbour shells used as well as the number of recursion steps before termination (see the discussion on convergence by Haydock and coworkers [79–81] and Chakrabarti and Mookerjee [73]). The advantage with disordered systems is that the fine structure in the density of states is smoothed by disorder scattering and the convergence of recursion is much faster than in periodic solids. The results quoted in the paper were for six nearest-neighbour shells in augmented space and twelve steps of recursion after which the Beer–Pettifor terminator [82] was used to estimate the asymptotic part of the continued fraction expansion of the averaged Green function. Since the averaged density of states for disordered alloys is smoother and has less structure as compared with that for a periodic system, the convergence is faster.

The PAW potentials for Fe and Cr were generated by including their 3d states in the valence configuration. The core radii for the PAW potentials were 1.22 and 1.32 Å for Fe and Cr, respectively. $4 \times 4 \times 4$ Monkhorst–Pack mesh was used for summation of charge densities over the Brillouin zone. The plane wave cutoff energy was set to 400 eV. All the atoms in the quasi-random supercell were relaxed till the Hellman–Feynman force on each ion was less than 0.01 eV Å^{-1}.

In all three implementations, we have used the Perdew–Burke–Ernzerhof (PBE) exchange–correlation functional [83].

In most alloy systems where the constituents are not iso-electronic, there is always charge realignment on alloying. As a result, in the muffin-tin based methods, the atomic spheres which were neutral in the pure constituents may become charged and contribute a significant Madelung energy. The evaluation of this Madelung energy for ordered compounds is quite straightforward, but in a disordered alloy, where the charged spheres are randomly distributed on the lattice, estimating the Madelung energy accurately is not an easy problem. No completely satisfactory method is available to date. Kudrnovský and Drchal [84] have suggested using different atomic radii for the constituents in such a way that average total volume is conserved, maintaining the overlap below a threshold value (15%), *and* such that these spheres are approximately neutral on the average. This allows us to ignore the Madelung contribution. Not only does this procedure need us to vary the ratio of atomic radii of the constituents $r = R_A/R_B$ and is therefore very cumbersome, Ruban and Skriver [85] have shown that local environmental effects (beyond the CPA) destroys the strict charge-potential alignment, and hence the possibility of choosing electro-neutral atomic spheres by a single ratio r. This has been discussed in detail earlier by us [86]. In an earlier work by us (Sanyal *et al* [87]) we had used this idea of electro-neutral atomic spheres to study FeCr. This earlier work did not observe any sign of the experimentally observed reversal of the Cr projected magnetic moment as a function of Fe concentration.

In this paper for two of the techniques (TB-LMTO-ASR and PAW-SQS) we have chosen the procedure of Ruban and Skriver [85] and define a one-electron potential as $V_i = -Q_i/R_{\text{av}}$, where i labels the constituents and Q_i is the net charge of the alloy component i in its own atomic sphere of average radius R_{av}. We use a single average atomic sphere radius for atoms. The Madelung energy is given by

$$E_{\text{Mad}} = \beta \frac{Q_i Q_j}{R_{\text{av}}}.$$

A *universal* parameter β has been proposed originally by Ruban and Skriver [85]. However, a much better estimate of this parameter may be obtained from a fit with an SQS calculation. In this latter, since it is a supercell calculation the estimation of Madelung energy is not difficult and the parameter β is obtained by comparison with these estimates. For the bcc lattice this value comes to 0.691 [88]. In that sense our TB-LMTO-ASR calculations will contain a part that is a marriage with the SQS method.

For the KKR-CPA we have used the 'charge correlated' model of Johnson and Pinski [89] for calculating the Madelung energy. The parameter β in the 'charge correlated' model is also taken as 0.691, which seems to be a universal parameter for the bcc lattice.

3. Electronic and magnetic structure of $\text{Fe}_x\text{Cr}_{1-x}$ alloys

3.1. Density of states

Our first step would be to examine the idea of spatial ergodicity in the application of the PAW-SQS method. We shall verify the convergence with cluster size, as suggested by Zunger *et al*

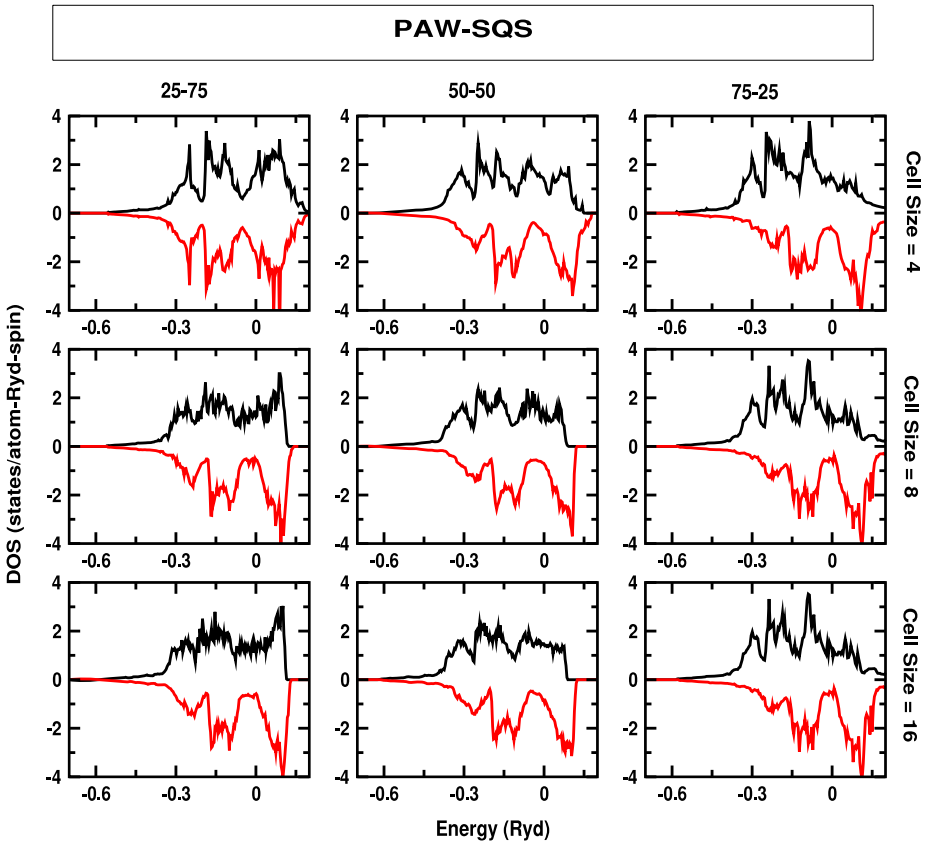

Figure 1. Density of states per spin for (left column) $Fe_{25}Cr_{75}$, (middle column) $Fe_{50}Cr_{50}$, (right column) $Fe_{75}Cr_{25}$, calculated by PAW-SQS with different sized quasi-random unit cells. Energies are measurements with respect to the Fermi energy ($E_F = 0$).

[64]. We have carried out calculations on SQS supercells of sizes 4, 8 and 16. Some results for three compositions are shown in figure 1. These DOS are averaged over all the different atoms in the cluster. We clearly see the eventual convergence of the results with supercell size. The 16-atom cluster is sufficient for our accuracy needs. We also note that there is considerable fine structure in the DOS. We shall argue later that this fine structure is an artefact of the finite supercell. For comparison with our other bulk calculations we shall smooth the raw SQS DOS using a Lorentzian broadening with a small width.

Figure 2 compares the density of states for the spin-up and spin-down states for Fe_xCr_{1-x} for compositions 25–75, 50–50 and 75–25 at which the solid solutions in the bcc lattice and the ferromagnetic state are stable at low temperatures. All three methods, KKR-CPA, TB-LMTO-ASR and PAW-SQS, were carried out within the LSDA self-consistency with the same Ceperley–Alder exchange correlation functional with Perdew–Zunger parametrization. The densities of states for both approaches show remarkable similarities. The corrections going beyond the CPA are small as compared with those in our earlier work on Cu_xZn_{1-x} [90].

Of course there are differences in detail. The KKR-CPA is a reciprocal-space-based approach while the TB-LMTO-ASR is a real-space-based one and the approximations in the two cases are different. The KKR-CPA is based on a single-site mean-field and relevant Brillouin zone integration involves techniques like tetrahedron integration. The TB-LMTO-ASR expands the configuration-averaged Green function as a continued fraction and the main approximation involves calculation of its asymptotic 'terminator'. As compared with an earlier work on Cu_xZn_{1-x} [90], where the ASR showed considerable improvement over the CPA, in this particular alloy system the differences are less prominent, except in the very dilute limit. This is an important observation, and we should be careful in making general and strong statements about the efficiency of one method over the other.

The middle column shows the PAW-SQS DOS for all three compositions. The raw DOS data in the SQS has considerable microstructure as compared to the CPA or ASR. We believe, as stated earlier, that these structures are artefacts of the supercell translational symmetry. The imaginary part of the self-energy which arises due to disorder scattering in the CPA or ASR is *per se* absent in SQS calculations. This 'lifetime' effect smooths the CPA or ASR density of states and gives it a larger width as compared to the SQS. If we enlarge the supercell to sizes larger than 16 (which we have used here) or carry out the calculations for more k points in the Brillouin zone, we expect the differences to be less prominent. The results shown here are smoothed by giving a small imaginary part to the energy.

Although the densities of states for all three techniques are very similar, it would be interesting to study their shapes in greater detail. Haydock [79], in his critique of the recursion method, argued that the density of states is perhaps not the

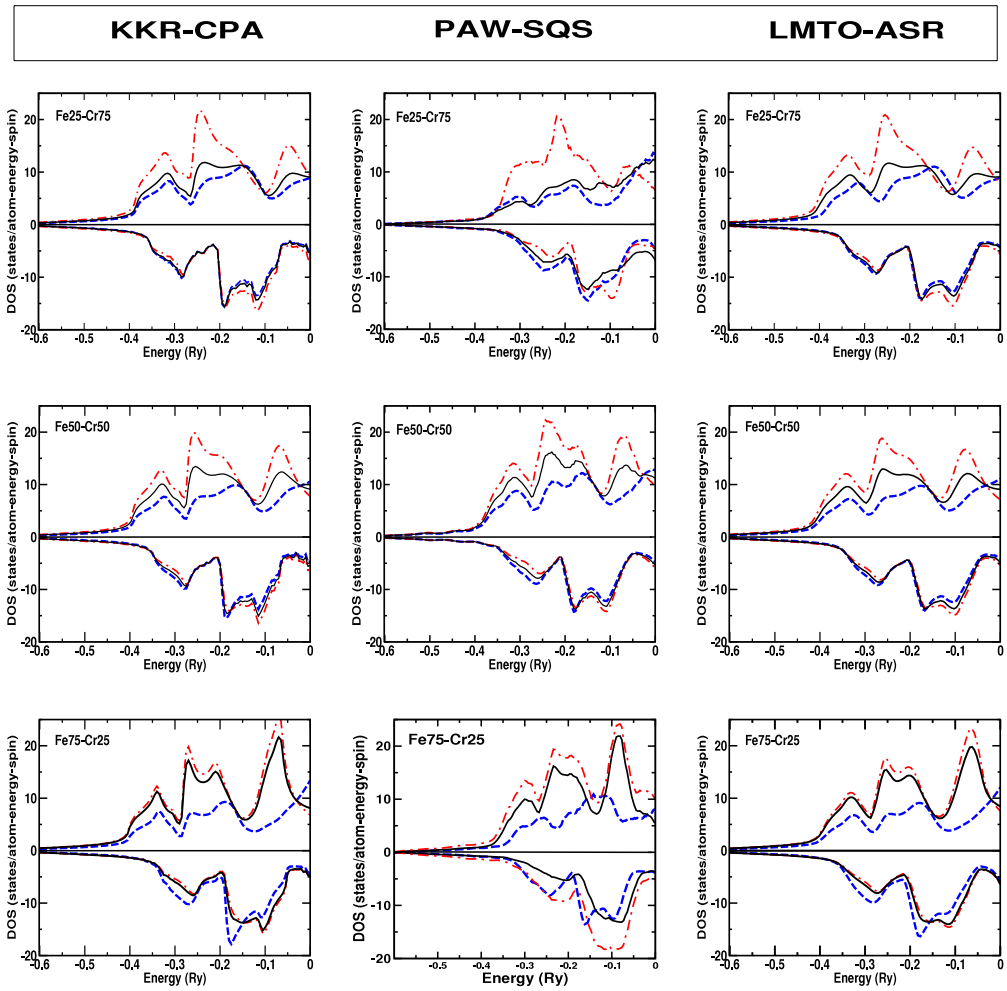

Figure 2. Element projected and total densities of states for the spin-up states (upright curves) and spin-down states (inverted curves) for Fe_xCr_{1-x}: red, dotted–dashed curves are for Fe projected DOS, blue dashed curves for Cr projected DOS and black full curves are the total DOS. Results are shown for various compositions: (top row) 25–75, (middle row) 50–50 and (bottom row) 75–25 in the ferromagnetic, bcc, disordered phase. The energies are shown with respect to the Fermi level as the reference level. The left columns are calculated using KKR-CPA, the middle column PAW-SQS and the right column TB-LMTO-ASR. The SQS DOS are smoothed by giving the energy a small imaginary part 0.01 Ryd. All energies are measured from the Fermi energy.

best property to compare between different approximations, because it is unstable to small perturbations. Thouless [91] has argued that the spectral density arising out of extended states in a disordered system is extremely sensitive to small perturbations. Minor differences in approximations lead to relatively large changes in the spectral density. Haydock suggested that it would be more proper to compare integrated *moment* functions like $M^n(E) = \int_{-\infty}^{E} \mathrm{d}E'(E')^n\, n(E')$. Examples are the integrated density of states, the Fermi and band energies and the various energy moments of the density of states. In fact, most physical properties are integrated functions of this kind.

Figure 3 shows the first three moments of the density of states $M_n(E) = \int_{-\infty}^{E} \mathrm{d}E' E'^n\, n(E')$ with $n = 0, 1, 2$. Since $M_0(E)$ is the integrated DOS, $M_0(E_\mathrm{F})$ is the same for all three methods. The moments match well throughout the energy range up to the Fermi energy with the relative deviations being no more than 10% throughout the energy range of interest. We notice, of course, a systematic trend between the three techniques. The SQS always gives a density of states which is narrower than the CPA or ASR. This is clear from the second moment function. Also, the ASR gives density of states distributed wider in energy than either the CPA or SQS. We believe this is because it includes correlated disorder scattering from clusters which is absent in the CPA and contributes to the self-energy. Simply from the density of states there is little to choose between the different methods.

To understand why all three methods work well for FeCr but only the ASR and SQS gave accurate results for CuZn, let us look at figure 4 which shows the spin and constituent projected DOS for $Fe_{50}Cr_{50}$. The projected DOS show rather interestingly that for the down-spin electrons the positions of the centres of the d-bands of Fe and Cr are almost degenerate and strongly hybridize. However, the d-bands of the up-spin electrons are separated in energy. FeCr is then only a partially split-band alloy. This implies that for the up-spin electrons the 'electrons travel more easily between Fe or between Cr sites than between unlike ones' [75]. So when the alloy

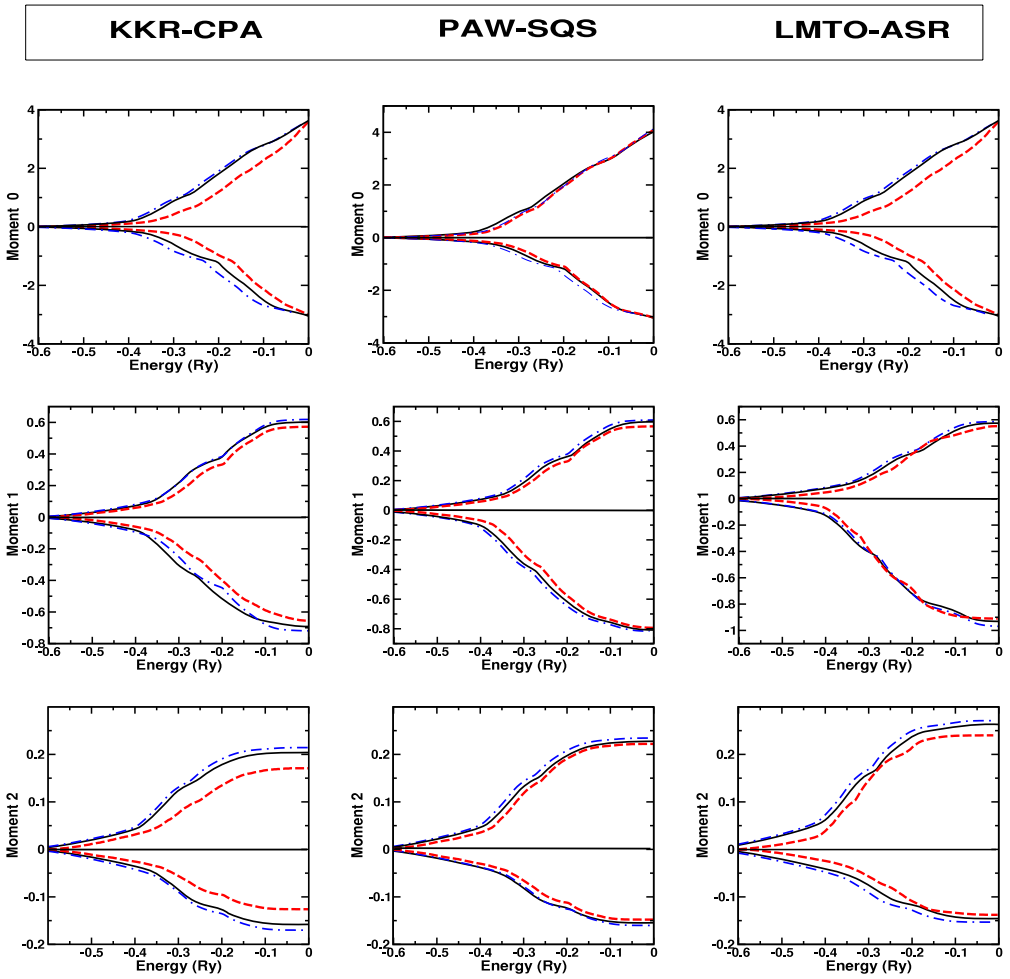

Figure 3. The first three moment functions for three compositions of Fe_xCr_{1-x}: (left column) 25–75, (middle column) 50–50, (right column) 75–25. The top row gives M^0, the middle row M^1 and the bottom row gives M^2. In each panel the dashed curves are PAW-SQS, the dashed–dotted curve TB-LMTO-ASR and the full curve KKR-CPA. All energies are measured from the Fermi energy.

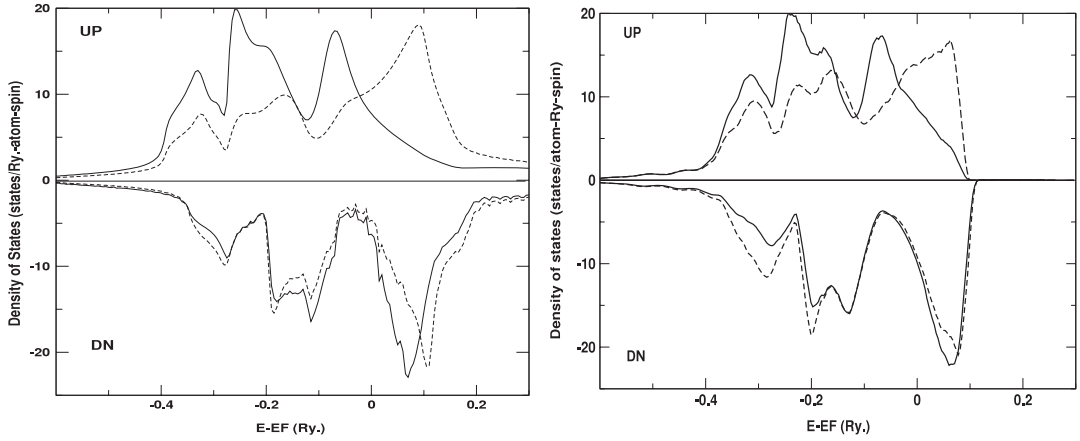

Figure 4. Spin and component projected DOS for $Fe_{50}Cr_{50}$ calculated by (left) TB-LMTO-ASR and (right) PAW-SQS. The SQS DOS are smoothed by giving the energy a small imaginary part 0.01 Ryd. All energies are measured from the Fermi energy.

orders and unlike sites sit next to each other, the overlap integral between the unlike sites is lower, and for up-spin the density of states narrow. For the down-spin bands this effect is not present. CuZn alloy is a fully split-band one, and it is in the dilute limit of such alloys that CPA is known be inaccurate.

It would be interesting to see how far our theoretical predictions of the densities of states are supported by

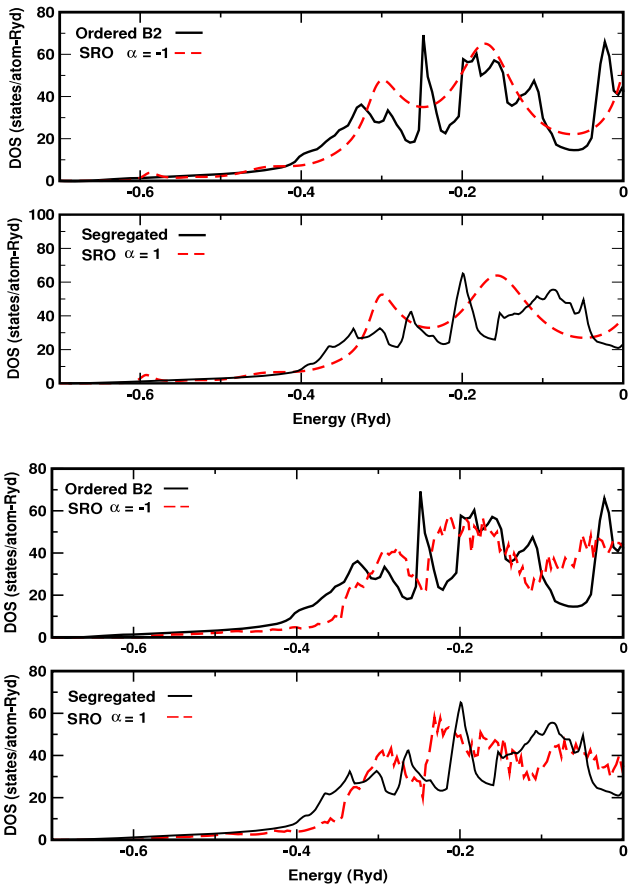

Figure 5. (Top) Density of states calculated from TB-LMTO-ASR for $\alpha = -1$ (dashed lines) compared with that of the ordered B2 structure (full lines) and for $\alpha = 1$ (dashed lines) compared with the segregated pure Fe and pure Cr density of states (full lines). (Bottom) The same as above, calculated from the PAW-SQS. Ordered and segregated calculations were done by TB-LMTO. All energies are measured from the Fermi energy.

experiments. Valence band spectroscopic studies on bulk FeCr alloys have been rare. There have been x-ray photoelectron spectra (XPS) studies by Terebova *et al* [92] on $Fe_{86}Cr_{14}$. If we look at figure 1 of the above-referenced article [92], which shows the XPS intensity variation with binding energy, the characteristic peaked structures at energies 0.04, 0.1, 0.17 and 0.25 Ryd may be compared with the peaked structures in our valence band density of states shown in our figure 2. More common is photo-emission spectroscopy (PES) on spinels based on FeCr as a building block. These show giant magnetoresistivity and hence are of interest. Examples are $FeCr_2S_4$ and $Fe_{0.5}Cu_{0.5}Cr_2S_4$ [93]. The structure of chalcogenide spinels differs from the bcc and there are extra constituents. Therefore we expect it would be difficult to compare these experimental results with our theoretical data. However, the main signature structures due to the Fe and Cr d states near the Fermi level, as seen from our theoretical calculations, are also evident from figures 3 and 5 of the work by Kang [93].

3.2. Short-ranged ordering

The phase diagram of Fe–Cr is simple at high temperatures [94] and a complete range of bcc solid solutions exists from 1093 K to the solidus. Alloys quenched from these temperatures retain their bcc structure. However, the alloys are not homogeneously disordered. Neutron scattering experiments [41] indicate that short-ranged clustering exists in these quenched alloys, leading to a miscibility gap at temperatures lower than 793 K. The single-site CPA cannot deal with short-ranged order as the latter explicitly involves independent scattering from more than one site. Attempts to develop generalizations of the coherent potential approximation (CPA) including effects of short-ranged order (SRO) have been many, spread over the last several decades. Many of them fail the analyticity test. Mookerjee and Prasad [95] generalized the augmented space theorem to include correlated disorder. However, since they then went on to apply it in the cluster CPA approximation, they could not go beyond the two-site cluster and that too only in model Hamiltonians. The breakthrough came with the augmented space recursion (ASR) approach proposed by Saha *et al* [96, 97]. The method was a departure from the mean-field approaches which always began by embedding a cluster in an effective medium which was then obtained self-consistently. As discussed earlier, here the Green function was expanded in a continued fraction whose asymptotic part was obtained from its initial steps through an ingenious *termination* procedure [79]. In this method the effect at a site of quite a large environment around it could be taken into account depending how far one went down the continued fraction before *termination*. The technique was made fully LDA-self-consistent within the TB-LMTO approach [73] and several applications have been carried out to include short-ranged order in different alloy systems [86]. Details of the formalism has been described in detail in an earlier paper [90].

We have already stated that the aim of this paper is to compare the three techniques KKR-CPA, TB-LMTO-ASR and PAW-SQS. For uncorrelated disorder we have seen that, although there are differences in detail, the three techniques give almost similar results. However, when SRO is taken into account, the CPA is unable to handle this problem since it is a single-site approximation. We shall, therefore, compare the TB-LMTO-ASR and PAW-SQS for Fe_xCr_{1-x} in the 50–50 composition. Construction of quasi-random structures including SRO has been described earlier by Zunger and coworkers. We have used the 16-atom supercell for these calculations.

We have carried out the TB-LMTO-ASR and PAW-SQS calculations on $Fe_{50}Cr_{50}$ including short-ranged ordering described by the nearest-neighbour Warren–Cowley parameter $\alpha(-1 \leqslant \alpha \leqslant 1)$. The Fe and Cr potentials are self-consistently obtained via the LSDA self-consistency loop. The same exchange–correlation functional was used as for the uncorrelated disorder case for both methods. All reciprocal-space integrals were carried out by using the generalized tetrahedron integration for disordered systems introduced by us earlier [98].

The second and fourth panels in figure 5 show the density of states with $\alpha = 1$ (dashed curves) using the TB-LMTO-ASR

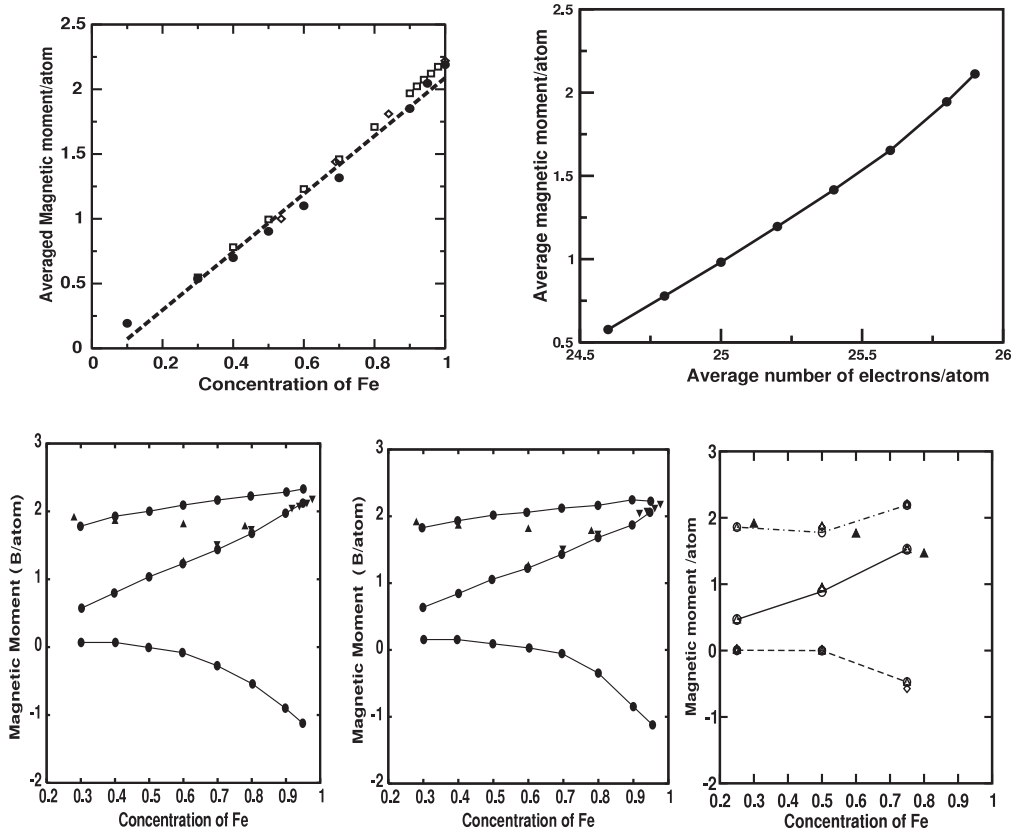

Figure 6. (Top panel, left) Compendium of experimental results on the averaged magnetic moment in Fe_xCr_{1-x}. The dashed line is fitted to the TB-LMTO-ASR results. (Top, right) Average magnetic moment in Fe_xCr_{1-x} as a function of the average number of electrons per atom. These are from the TB-LMTO-ASR work. (Bottom panel) Local moments on Fe and Cr and average magnetic moment in Fe_xCr_{1-x} as functions of composition. (Left) from TB-LMTO-ASR, (middle) from KKR-CPA, (right) from PAW-SQS. The filled circles are theoretical results, while filled triangles and inverted triangles are experimental data.

and PAW-SQS, respectively. Positive α indicates a clustering or segregating tendency. Compare these with the full curves which are a concentration-weighted sum of the density of states of Fe and Cr. We note first that there is a close resemblance between the ASR and SQS results. For $\alpha = 1$ there is still residual long-ranged disorder. This causes smoothing of the bands with respect to the pure materials. The weighted sum DOS ignores the intra-cluster interactions: as a result, some of its structures like the peak at -0.2 Ryd below E_F appear to be shifted and are not well reproduced by the SRO DOS by either of the two techniques.

The top and third panels in figure 5 show the density of states with $\alpha = -1$ (dashed curves) using the TB-LMTO-ASR and PAW-SQS, respectively. $\alpha = -1$ indicates nearest-neighbour ordering. On the bcc lattice at 50–50 composition we expect this ordering to favour a B2 structure. We can compare the SRO results with the density of states for the B2 structure shown as full curves. Here the ASR seems to reproduce the dip in the DOS around -0.05 Ryd below the Fermi energy better than the SQS. We have to realize that, as we have taken only the nearest-neighbour short-ranged order, $\alpha = -1$ does not imply perfect long-ranged ordering. Thus the detailed structure, like the sharp peak at -0.25 Ryd below the Fermi energy, is not reproduced, while the several structures between -0.1 and -0.2 Ryd below the Fermi energy are smoothed into a large humped structure.

3.3. Magnetic moments

Experimental work on magnetism in Fe_xCr_{1-x} alloys has a long history [29, 41, 42, 99–101]. A series of theoretical approaches using different electronic structure methods and usually the CPA followed the experiments [56, 57, 59, 4]. Finally, Cieślak *et al* [43] gathered together results for both the Curie temperature and the average magnetic moment from resistivity minima [45], specific heat anomaly [44] and elastic measurements [102]. A compendium of the acceptable experimental results on the average magnetic moments for different compositions is shown in figure 6 (top left). Results from different experiments are shown by different symbols. The TB-LMTO-ASR theoretical results which fit the curve $m(x) = 2.44x - 0.244$ is shown by the dashed curve. The KKR-CPA and PAW-SQS predictions for the total magnetic moment per atom are almost the same. The theoretical predictions from all these methods agree well with the experimental results.

Figure 6 (bottom panel) shows the variation of the local and average magnetic moment as a function of Fe concentration of the alloy studied from the KKR-CPA, TB-LMTO-ASR and PAW-SQS methods. The results are in

good agreement with the few experimental observations available. They show that the local Fe moment with increasing Fe concentration remains almost constant over the entire concentration range while the Cr moment changes its sign ($x > 0.4$) from low positive value to very high negative value. Earlier studies have also observed similar behaviour. The KKR-CPA and TB-LMTO-ASR are in good agreement for the Fe local magnetic moment, while the agreement is less close for the local moment on Cr. Unfortunately, there are no experimental data on the local moment on Cr. This is in contrast to the much better reproduction by the TB-LMTO-ASR of the local moment on Ni in Ni-based alloys, as compared to the CPA. This is because the fragile moment of Ni is dependent strongly on its immediate neighbourhood, which cannot be adequately described by the single-site CPA [86]. The moment on Cr is less dependent on the configuration of its immediate neighbourhood and the CPA here is not a bad description. We note that the experimental dip in the local magnetic moment at 50–50 composition is much better reproduced by the PAW-SQS than the other two methods. Both the ASR and the SQS show a more rapid increase in the negative local moment of Cr than the CPA for higher concentrations of Fe.

From figure 2 we see that the Fermi energy is pinned to the minimum of the minority spin density of states. But for $x > 0.5$ the majority spin density of states is entirely filled. It shows that, with increasing Fe concentration, the additional electrons are added mainly to the spin-up d band. As we scan through the concentration range the Cr spin-up density of states shows major ($x > 0.7$) variation. This is understandable as we see that initially, for low x compositions, Cr d-up orbitals tend to acquire more charge than d-down ones, but for $x > 0.5$ compositions the reverse phenomenon is observed. In our calculation this is the critical concentration at which the Cr projected magnetic moment reverses its sign.

Figure 6 (top right panel) shows the variation of average magnetic moment against the average number of electrons. This is the Slater–Pauling curve and it shows an almost linear variation up to $x = 0.8$, above which the Cr moment changes very rapidly to larger negative values. This observation is in accordance with earlier studies.

4. Summary

We have used three different techniques for the calculation of the electronic structure of fully disordered Fe_xCr_{1-x} alloys: the KKR-CPA, the TB-LMTO-ASR and the PAW-SQS. Each of the methods have their own distinct approximations and the aim was to determine, for this specific alloy system, their suitability and relative accuracy. Unlike the earlier study of Cu_xZn_{1-x} [90], we find agreement in the shapes of the density of states and their energy moments for all three techniques. The local and averaged magnetic moments are also very similar, except for the Cr local moments in the dilute Cr limit. Unfortunately, experimental data for the Cr local moment in this limit was not available. The difference in the average magnetic moment in the dilute limit between KKR-CPA, PAW-SQS and TB-LMTO-ASR is too small to warrant comment.

The single-site CPA cannot effectively address the problem of short-range ordering. Neutron scattering experiments on Fe_xCr_{1-x} alloys indicate a degree of short-ranged ordering. Both the generalized ASR and the SQS can tackle this problem. We have shown that, again, within our error windows, the results of the ASR and SQS over the variation of the Warren–Cowley SRO parameter are also very similar.

Finally, as mentioned earlier, despite lattice matching between Fe and Cr, local bond lengths are dependent on the environment. Such local lattice distortions cannot be addressed by the CPA. We had earlier shown that the ASR can address the problem of local lattice distortions due to alloying [103]. However, in its actual implementation only random variation of bond lengths due to such distortions was taken into account. Topological distortions over plaquettes of atoms were discussed but were rather cumbersome to include in the calculations. It is here that the SQS really wins over other techniques. It can include random distortions of bond angles as well within the quasi-random supercell.

Acknowledgment

KT would like to thank the CSIR for financial support during the time this work was carried out. AM, BS and OE would like to thank the Sweden-Asia Research Link Programme for support of the project under which this work was carried out. They also thank the Department of Materials Science, Ångström Laboratariet, Uppsala University for hospitality during the completion of this work. BS acknowledges computational support from the Swedish National Infrastructure for Computing (SNIC).

References

[1] Froideval A, Iglesias R, Samaras M, Schuppler S, Nagel P, Grolimund D, Victoria M and Hoffelner W 2007 *Phys. Rev. Lett.* **99** 237201
[2] Cook I 2006 *Nat. Mater.* **5** 77
[3] Kubik M, Handke B, Karaś W, Spiridis N, Ślezak T and Korecki J 2002 *Phys. Status Solidi* a **189** 705
[4] Qiu S L, Moruzzi V L and Marcus P M 1999 *J. Appl. Phys.* **85** 4839
[5] Brenner S S, Miller M K and Soffa W A 1982 *Scr. Metall.* **16** 831
[6] Curvich L V, Veits I V, Medvedev V A, Bergman G A and Yungnan V S 1982 *Thermodynamic Properties of Individual Substances* vol 4 (Moscow: Nauka) part I p 9
[7] Hertzman S and Sundman B 1982 *Calphad* **6** 67
[8] Iguchi Y, Nobori S, Saito K and Fuwa T 1982 *Tetsu-to-Hagane* **68** 633
[9] Vilar R M and Cizeron G 1982 *Mem. Etud. Sci. Rev. Metall.* **79** 687
Vilar R M and Cizeron G 1983 *J. Mater. Sci. Lett.* **2** 283
[10] Batalin G I, Kurach V P and Sudavtseva V S 1984 *Russ. J. Phys. Chem.* **58** 289
[11] De Nys T and Gielen P M 1971 *Metall. Trans.* **2** 1423
[12] Kirchner G, Nishizawa T and Uhrenius B 1973 *Metall. Trans.* **4** 167
[13] Mazandarany F N and Pehlke R D 1973 *Metall. Trans.* **4** 2067
[14] Williams R O 1974 *Metall. Trans.* **5** 967

[15] Langer S, Bar-on M and Miller H D 1975 *Phys. Rev.* A **11** l417
[16] Babynk T I, Kushta G,P and Chomey S A 1973 *Phys. Met. Metallogr.* **35** 176
[17] Babynk T I, Kushta G P and Rybailo O I 1974 *Izv. Vyssh. Uchebn. Zaved. Chernaya Metall.* **7** 126
[18] Katarro S and Iizumi M 1982 *J. Phys. Soc. Japan* **2** 347
[19] Swan-Wood T L, Delaire O and Fultz B 2005 *Phys. Rev.* B **72** 024305
[20] Chandra D and Schwartz L H 1971 *Metall. Trans.* **2** 511
[21] Dunlap B D, Aldred A T, Nemanich R J and Kimball C W 1976 *AIP Conf. Proc.* **29** 232
[22] Makarov V A, Puzey I N, Koropiy A N and Sakharova T V 1982 *Phys. Met. Metallogr.* **54** 66
[23] Dubiel S M and Inden G 1987 *Z. Metallkd.* **78** 544
[24] Cieślak J, Reissner M, Steiner W and Dubiel S M 2003 *J. Magn. Magn. Mater.* **272–276** 534
[25] Downie D B and Martin J F 1984 *J. Chem. Thermodyn.* **16** 743
[26] Polovov V M 1974 *Sov. Phys.—JETP* **39** 1064–71
[27] Maclnnes W M and Schröder K 1972 *Proc. Conf. on Dynamical Aspects of Critical Phenomena* p 305
[28] Arajs S and Anderson E E 1971 *Physica* **54** 617
[29] Matthews J C and Morton N 1965 *Proc. Phys. Soc.* **85** 343
[30] Burke S K and Rainford B D 1983 *J. Phys. F: Met. Phys.* **13** 441
[31] Burke S K, Cywinski R, Davis J R and Rainford B D 1983 *J. Phys. F: Met. Phys.* **13** 451
[32] Burke S K and Rainford B D 1983 *J. Phys. F: Met. Phys.* **13** 471
[33] Dorofeyev Yu A, Men'shikov A Z and Takzey G A 1983 *Phys. Met. Metallogr.* **55** 102
[34] Palumbo A C, Parks R D and Yeshurun Y 1983 *J. Magn. Magn. Mater.* **36** 66
[35] Aldred A T and Kouvel J S 1985 *Physica* B **86–88** 5
[36] Gomankov V I, Zaitsev A I, Puzei I M and Tretyakov B N 1988 *Sov. Phys.—JETP* **68** 1462
[37] Kordyr A I, Borisnyk A and Yur'ev S A 1990 *Phys. Met. Metallorg.* **69** 128
[38] Beck P A 1991 *Phys. Rev.* B **44** 7115
[39] Murugesan M, Chikazawa S and Kuwano H 1999 *HC04: Magnetism Conf., IEEE Int.*
[40] Fischer S F, Kaul S N and Kronmüller H 2001 *J. Magn. Magn. Mater.* **226–230** 540
[41] Aldred A T 1976 *Phys. Rev.* B **14** 216
[42] Shull C H and Wilkinson M K 1955 *Phys. Rev.* **97** 304
[43] Cieślak J, Reisser M, Steiner W and Dubiel S M 534 *J. Magn. Magn. Mater.* **272–276** 534
[44] Wei C T and Cheng C H 1961 *Phys. Rev.* **124** 722
[45] Newman M M and Stevens W H 1959 *Proc. R. Soc.* **74** 290
[46] Rao M V and Tiller W A 1974 *Mater. Sci. Eng.* **14** 47
[47] Andersson J-O and Sundman B 1987 *Calphad* **11** 83
[48] Chuang Y-Y, Lin J-C and Chang Y A 1987 *Calphad* **11** 57
[49] Rao M V and Tiller A 1972 *Scr. Metall.* **6** 417
[50] Katano S and Iizumi M 1983 *Physica* B **120** 392
[51] Kuwano H 1985 *Japan. Int. Met.* **26** 473
[52] Furusaka M, Ishikawa Y and Mera M 1985 *Phys. Rev. Lett.* **54** 264
[53] Batalev G I, Kurach V P and Sudavtseva V S 1984 *Russ. J. Phys. Chem.* **58** 289
[54] Moruzzi V L, Marcus P M and Pattanaik P C 1988 *Phys. Rev.* B **37** 8003
[55] Moruzzi V L and Marcus P M 1990 *Phys. Rev.* **42** 8361
Moruzzi V L and Marcus P M 1992 *Phys. Rev.* B **46** 14198
[56] Moroni E G and Jarlborg T 1993 *Phys. Rev.* B **47** 3255
[57] Singh D J 1994 *J. Appl. Phys.* **75** 6688
[58] Sluiter M H F, Esfarjani K and Kawazoe Y 1995 *Phys. Rev. Lett.* **75** 3142
[59] Moriatis G, Khan M A, Dreysee H and Demangeat C 1996 *J. Magn. Magn. Mater.* **156** 250
[60] Butler W H, Zhang X and MacLaren J M 1998 *MMM-Intermaq Conf.* p 301
[61] Dederichs P H, Zeler R, Akai H and Ebert H 1991 *J. Magn. Magn. Mater.* **100** 247
[62] Kulikov N I and Demangeat C 1997 *Phys. Rev.* B **55** 3533
[63] Jiang C, Wolverton C, Sofo J, Chen L-Q and Liu Z-K 2004 *Phys. Rev.* B **69** 214202
[64] Zunger A, Wei S-H, Ferreira L G and Bernard J 1990 *Phys. Rev. Lett.* **65** 353
[65] Olsson P, Abrikosov A and Wallenius J 2006 *Phys. Rev.* B **73** 104416
[66] Turchi P E A, Reihard L and Stocks G M 1994 *Phys. Rev.* B **50** 15542
[67] Mookerjee A 2003 *Electronic Structure of Alloys, Surfaces and Clusters* ed D D Sarma and A Mookerjee (London: Taylor and Francis)
[68] Kresse G and Haffner J 1993 *Phys. Rev.* B **47** 558
[69] Kresse G and Furthmüller J 1996 *Comput. Mater. Sci.* **6** 15
[70] Kresse G and Joubert D 1999 *Phys. Rev.* B **59** 1758
[71] Blöchl P E 1994 *Phys. Rev* B **50** 17953
[72] Ghosh S, Leath P L and Cohen M H 2002 *Phys. Rev.* B **66** 214206
[73] Chakrabarti A and Mookerjee A 2005 *Eur. Phys. J.* B **44** 21
[74] Jarrell M and Krishnamurthy H R 2001 *Phys. Rev.* B **63** 125102
[75] Rowlands D A, Staunton J B, Gyorffy B L, Bruno E and Ginatempo B 2005 *Phys. Rev.* B **72** 045101
[76] Johnson D D, Nicholson D M, Pinski F J, Stocks G M and Gyorffy B L 1990 *Phys. Rev.* B **41** 9701
[77] Smirnov A V and Johnson D D 2002 *Comput. Phys. Commun.* **148** 74
[78] Johnson D D, Nicholson D M, Pinski F J, Gyorffy B L and Stocks G M 1986 *Phys. Rev. Lett.* **56** 2088
[79] Haydock R 1980 *Lecture Notes in Physics* vol 35 (New York: Academic)
[80] Haydock R 1981 *Phil. Mag.* B **43** 203
Haydock R and Te R L 1994 *Phys. Rev.* B **49** 10845
[81] Haydock R 1972 *Thesis* University of Cambridge, UK
[82] Beer N and Pettifor D G 1982 *The Electronic Structure of Complex Systems* vol 113, ed P Phariseau and W M Temmerman (New York: Plenum) p 769
[83] Perdew J P, Chevary J A, Vosko S H, Jackson K A, Pederson M R, Singh D J and Fiolhais C 1999 *Phys. Rev.* B **46** 6671
[84] Kudrnovský J and Drchal V 1990 *Phys. Rev.* B **41** 7515
[85] Ruban A V and Skriver H L 2003 *Phys. Rev.* B **66** 024201
[86] Paudyal D, Saha-Dasgupta T and Mookerjee A 2004 *J. Phys.: Condens. Matter* **16** 2317
[87] Sanyal B, Basu Chaudhuri C and Mookerjee A 2002 *Physica* B **14** 3211
[88] Korzhavyi P A, Ruban A V, Abrikosov I A and Skriver H L 1995 *Phys. Rev.* B **51** 5773
[89] Johnson D D and Pinski F J 1993 *Phys. Rev.* B **48** 11553
[90] Tarafder K, Chakrabarti A, Saha K K and Mookerjee A 2006 *Phys. Rev.* B **74** 144204
[91] Thouless D 1974 *Phys. Rep.* **13** 93
[92] Terebova N S, Shabanova I N and Makhneva T M 1998 *J. Electron Spectrosc. Relat. Phenom.* **88–91** 449
[93] Kang J-S, Kim S J, Kim C S, Olson C G and Min B I 2003 *Phys. Rev.* B **63** 144412
[94] Elliot R 1970 *Structures of Binary Alloys* (Moscow: Metallurgiya)
[95] Mookerjee A and Prasad R 1993 *Phys. Rev.* B **48** 17724

[96] Saha T, Dasgupta I and Mookerjee A 1994 *Phys. Rev.* B **50** 13267
[97] Saha T, Dasgupta I and Mookerjee A 1996 *J. Phys.: Condens. Matter* **8** 1979
[98] Saha K K, Mookerjee A and Jepsen O 2005 *Phys. Rev.* B **71** 094207
[99] Fallot M 1936 *Ann. Phys. (Paris)* **6** 305
[100] Hasegawa H and Kanamori J 1972 *J. Phys. Soc. Japan* **33** 1607
[101] Frolliani G, Menzinger F and Sachetti an F 1975 *Phys. Rev.* B **11** 2030
[102] De Morton M E 1963 *Phys. Rev. Lett.* **10** 208
[103] Saha T and Mookerjee A 1996 *J. Phys.: Condens. Matter* **8** 2915